



Cite this: *Phys. Chem. Chem. Phys.*,
2018, 20, 7593

Understanding proton capture and cation-induced dimerization of $[\text{Ag}_{29}(\text{BDT})_{12}]^{3-}$ clusters by ion mobility mass spectrometry†

Papri Chakraborty,^{‡a} Ananya Baksi,^{‡§a} Sathish Kumar Mudedla,^b Abhijit Nag,^a
Ganesan Paramasivam,^a Venkatesan Subramanian^{ib} and Thalappil Pradeep^{id*}

Proton transfer reactions have been a topic of fundamental interest in several areas of chemistry and biology. However, such reactivity has not been explored in detail for nanoscale materials. In this article, we present a unique reaction of an atomically precise monolayer-protected silver nanocluster, $[\text{Ag}_{29}(\text{BDT})_{12}]^{3-}$, with a proton (H^+). Under controlled conditions, the strong proton affinity facilitated a complete conversion of the cluster to its protonated form, $[\text{Ag}_{29}(\text{BDT})_{12}\text{H}]^{2-}$. Moreover, binding of alkali metal ions (Li^+ , Na^+ , K^+ , Rb^+ and Cs^+) induced specific structural changes and also favored dimerization of the cluster. In this case, the cations acted as a bridge between the two clusters and the degree of dimerization was specific to the size of the cations. The conformational changes and separation of the alkali-metal ion bound dimers from their respective monomers have been investigated by ion mobility mass spectrometry (IM MS) and tandem mass spectrometric studies. Density functional theory (DFT) calculations have been used to determine the possible structures of the monomers and the dimers. Similar reactivity of the cluster can also be extended to other metal ions. While the present study helps to expand the ion-chemistry of atomically precise clusters, gas-phase basicity of the molecule can be explored in further detail and this can find applications in the areas of sensing and materials in general.

Received 6th December 2017,
Accepted 12th February 2018

DOI: 10.1039/c7cp08181b

rs.li/pccp

1. Introduction

Monolayer-protected clusters are emerging as an interesting family of nanomaterials. These nanoscale materials are becoming increasingly important due to their structures, diverse properties, and widespread applications.^{1–5} Condensed phase science of these clusters is expanding in different directions due to their potential applications in sensing, catalysis, imaging, *etc.* Up to now, several clusters have been crystallized and their structures have been solved by X-ray crystallography. Some of the noted examples are clusters like $\text{Au}_{25}(\text{SR})_{18}$,⁶ $\text{Au}_{38}(\text{SR})_{24}$,⁷ $\text{Au}_{102}(\text{SR})_{44}$,⁸ $\text{Ag}_{44}(\text{SR})_{30}$,⁹ $\text{Ag}_{25}(\text{SR})_{18}$,¹⁰ $\text{Ag}_{29}(\text{S}_2\text{R})_{12}$,¹¹ *etc.* These clusters are well characterized by distinct absorption features

and also by mass spectrometry. Isotope patterns obtained from high resolution mass spectrometric techniques have helped to identify their molecular formulae and hence the exact composition of the clusters in the gas phase. Solution-phase properties of the clusters have been studied for a long time. However, gas-phase studies provide new insights into understanding their properties, and recently such studies have become important.^{12–15} Another emerging field is intercluster reactions.¹⁶ Detection of intermediate products helps to understand the reaction mechanism.¹⁷ Several interactions like H-bonding, van der Waals forces, and dipole-dipole interactions exist and they can result in the formation of different types of adducts of clusters. $\text{Ag}_{44}(p\text{-MBA})_{30}$ (*p*-MBA is *para* mercapto benzoic acid) clusters remain hydrogen bonded to their neighboring ones in their superlattice structures.¹⁸ Such interactions are important in controlling highly precise cluster-mediated self-assemblies.¹⁹ $\text{Au}_{25}(\text{SBu})_{18}$ (SBu is butane thiolate) is known to form a linear polymer in its crystal structure *via* Au–Au single bonds stabilized by appropriate orientation of the clusters.²⁰ An intercluster reaction between $[\text{Au}_{25}(\text{SR})_{18}]^-$ and $[\text{Ag}_{25}(\text{SR})_{18}]^-$ also involves the formation of a transient dianionic adduct, $[\text{Au}_{25}\text{Ag}_{25}(\text{SR})_{36}]^{2-}$.¹⁶ Polymeric forms of $[\text{Au}_{25}(\text{SR})_{18}]^-$ clusters have been detected in the gas phase.²¹ However, aurophilic interaction is one of the essential factors favoring such a dimerization process,

^a DST Unit of Nanoscience (DST UNS) and Thematic Unit of Excellence,
Department of Chemistry, Indian Institute of Technology Madras,
Chennai 600036, India. E-mail: pradeep@iitm.ac.in; Fax: +91-44 2257-0545

^b Chemical Laboratory, CSIR-Central Leather Research Institute, Adyar, Chennai,
600020, India

† Electronic supplementary information (ESI) available: Additional ESI MS,
UV-vis and computational details. See DOI: 10.1039/c7cp08181b

‡ These authors contributed equally.

§ Presently a postdoctoral fellow at Karlsruhe Institute of Technology (KIT),
Institute of Nanotechnology, Hermann-von-Helmholtz-Platz 1, 76344 Eggenstein-
Leopoldshafen, Germany.

which was reflected in the absence of any dimerization in the structurally similar $[\text{Ag}_{25}(\text{SR})_{18}]^-$ cluster. Similarly, $[\text{Ag}_{29}(\text{S}_2\text{R})_{12}]^{3-}$ also does not dimerize, possibly due to the lack of suitable interactions to favor such a process.

In this article, we present a new aspect of cluster dimerization mediated through cations. This is possibly due to additional interactions that arise in the system due to the incorporation of a new metal center. We have characterized and separated the dimers by ion-mobility mass spectrometry (IM MS). IM MS studies help in understanding the structure and conformational dynamics present in a system.²² Though such techniques have been used extensively to study proteins and macromolecules,^{23–27} recently these techniques have also become useful in the case of clusters.^{28,29} Reactivity of the cluster with a series of alkali metal ions (Li^+ , Na^+ , K^+ , Rb^+ and Cs^+) and their effect on the dimerization process have been studied. Ion-mobility and dissociation studies reflect the similarity in their structures. Such interactions can be expanded across a number of similar metals. Another aspect that is brought about in this article is the uniqueness of the interaction of the $[\text{Ag}_{29}(\text{BDT})_{12}]^{3-}$ cluster with protons. Interaction of hydrogen with $[\text{Au}_{25}(\text{SR})_{18}]$ clusters has been studied theoretically, which predicts that hydrogen can behave as a metal atom in the clusters and contribute its one electron to the superatomic free-electron count.³⁰ Hydride protected Ag, Cu and Fe clusters have also been characterized.^{31–34} Herein, we explore the reactivity of a proton (H^+) with the cluster $[\text{Ag}_{29}(\text{BDT})_{12}]^{3-}$. H^+ interacts with the cluster to form $[\text{Ag}_{29}(\text{BDT})_{12}\text{H}]^{2-}$. Affinity towards protons can give an idea regarding the gas-phase basicity of a molecule.^{35–39} Proton-transfer reactions are of immense importance in chemistry and in biomolecular processes.^{40–43} So, it has been an important area of research for years and such studies have been performed for a wide range of molecules starting from small molecules, amino acids, peptides and proteins. Structural changes resulting from the interaction of the cluster with a proton as well as alkali metal ions have been studied by density functional theory calculations. Computational studies are also presented to understand the possible structures for the dimers.

2. Experimental section

2.1 Reagents and materials

All the materials were commercially available and used without further purification. Silver nitrate (AgNO_3 , 99.9%) was purchased from Rankem, India. 1,3-Benzene dithiol (1,3-BDT), sodium borohydride (NaBH_4), and formic acid (98%) were purchased from Sigma Aldrich. Triphenylphosphine (TPP) was purchased from Spectrochem, India. Ammonium acetate (NH_4OAc), sodium acetate (NaOAc), lithium bromide (LiBr), potassium acetate (KOAc), rubidium bromide (RbBr) and cesium acetate (CsOAc) were purchased from Sigma Aldrich. All the solvents, dichloromethane (DCM), methanol (MeOH), ethanol (EtOH), acetonitrile (ACN) and dimethylformamide (DMF), were of HPLC grade and were used without further distillation.

2.2 Synthesis of the $[\text{Ag}_{29}(\text{BDT})_{12}(\text{TPP})_4]$ cluster

The $[\text{Ag}_{29}(\text{BDT})_{12}(\text{TPP})_4]$ cluster was synthesized following a reported protocol with slight modifications.¹¹ About 20 mg of AgNO_3 was dissolved in a mixture of 5 mL of methanol and 10 mL of DCM. To this reaction mixture, about 13.5 μL of 1,3-benzene dithiol (1,3-BDT) ligand was added. Then, the mixture was kept under stirring conditions. Shortly after this, 200 mg of TPP dissolved in 1 mL of DCM was added to the reaction mixture. The solution turned colorless indicating the formation of a Ag–S–P complex. After about 10 min, 10.5 mg of NaBH_4 dissolved in 500 μL of ice-cold water was added. Upon addition of NaBH_4 , the solution turned dark brown in color immediately. Gradually, the color changed to orange. Continuous stirring was carried out for 3 h under dark conditions. The reaction mixture was then centrifuged and the supernatant was discarded. The precipitate was washed twice with methanol and then dissolved in DMF and centrifuged. The precipitate was discarded and the supernatant contained the purified clusters dissolved in DMF.

2.3 Instrumentation

The UV-vis spectra were measured using a PerkinElmer Lambda 25 UV-vis spectrometer. Mass spectrometric measurements were carried out in a Waters Synapt G2–Si high definition mass spectrometer. The instrument is well equipped with electrospray ionization and ion mobility separation techniques. A concentration of about 1 $\mu\text{g mL}^{-1}$ was used for the cluster solution. Samples were infused at a flow rate of 20 $\mu\text{L min}^{-1}$. The source and desolvation temperatures were set at 100 $^\circ\text{C}$ and 200 $^\circ\text{C}$, respectively. Soft ionization conditions involving capillary voltage: 1.5 kV, cone voltage: 0 V, source offset: 0 V, source and desolvation temperature: 50 $^\circ\text{C}$, and desolvation gas flow rate: 100 L h^{-1} were used for preventing the TPP loss during the ionization and observing the intact TPP protected clusters.

2.4 Computational details

We used density functional theory (DFT) with projector augmented waves (PAWs) as implemented in GPAW.^{44,45} The PAW setup used was $\text{Ag}(4d^{10}5s^1)$, $\text{S}(3s^23p^4)$, $\text{C}(2s^22p^2)$, $\text{P}(3s^23p^3)$, $\text{H}(1s^1)$, $\text{Na}(3s^1)$ and $\text{Cs}(5s^25p^66s^1)$, with scalar-relativistic effects included for Ag. The PBE⁴⁶ functional and DZP (double zeta plus polarization) basis set were chosen in LCAO mode⁴⁷ to improve the efficiency of the calculations. The geometry optimizations were carried out with a grid spacing of 0.2 \AA and minimizing the residual forces without any symmetry constraints by 0.05 eV \AA^{-1} . The relative energies (REs) were calculated with respect to the most stable isomer. The binding energies of the cations to the cluster were calculated by subtracting the sum of the energies of the cluster $[\text{Ag}_{29}(\text{BDT})_{12}]^{3-}$ and M (M = H, Na *etc.*) from their respective complexes, $[\text{Ag}_{29}(\text{BDT})_{12}\text{M}]^{2-}$. The structures of the dimers have been optimized using the same level of theory as that used for the monomers.

3. Results and discussion

The $[\text{Ag}_{29}(\text{BDT})_{12}(\text{TPP})_4]^{3-}$ cluster was synthesized by the method described above (see Experimental section 2.2) and characterized using UV-vis and ESI MS (see Fig. S1, ESI†).¹¹ The cluster was

well characterized by distinct molecule-like features at 447 nm and 513 nm in its optical absorption spectra. In ESI MS, an intense peak was observed at m/z 1603, which corresponded to $[\text{Ag}_{29}(\text{BDT})_{12}]^{3-}$. The labile TPP ligands were lost during the ionization. The intact $[\text{Ag}_{29}(\text{BDT})_{12}(\text{TPP})_4]^{3-}$ cluster could be observed only under soft ionization conditions (Fig. S1C, ESI[†]). So, the gas-phase measurements and the related theoretical calculations have been performed primarily with $[\text{Ag}_{29}(\text{BDT})_{12}]^{3-}$ clusters.

3.1 Protonation of $[\text{Ag}_{29}(\text{BDT})_{12}(\text{TPP})_4]^{3-}$ clusters

It is known from previous reports that the $[\text{Ag}_{29}(\text{BDT})_{12}(\text{TPP})_4]^{3-}$ cluster¹¹ consists of an icosahedral Ag_{13} core protected by staple motifs consisting of Ag and S atoms. Though the core remains highly protected, the Ag and S atoms in the exterior shells may exhibit some selective affinity towards specific binding groups. The delocalized negative charge density of the cluster also imparts an affinity for binding with suitable positively charged counterparts. In an attempt to explore such reactivity, we studied the effect of the addition of cations to the cluster. As there are numerous S atoms exposed in the outer staples, they may interact with protons and induce some specific structural changes in the

system. Experiments were carried out by adding formic acid (a well-known proton donor) to the cluster solution and its reactivity was monitored carefully using ESI MS. A solution of about 0.1 mM cluster solution was prepared, and in the presence of about 1 mM formic acid in DMF, a peak at m/z 2406 started increasing in intensity. This is shown in Fig. 1A(a). The peak increased in intensity with increasing concentration of the acid (Fig. S2, ESI[†]) and became maximum when the formic acid concentration was around 12 mM (Fig. 1A(b)). However, the concentration of the acid could not be increased further to favor a complete conversion as, beyond this concentration of the acid, the cluster started to show degradation. Addition of formic acid changes the pH of the solution, it may also cause a change in the charge distribution of the cluster and all these factors can significantly affect the cluster stability. The new peak was assigned as $[\text{Ag}_{29}(\text{BDT})_{12}\text{H}]^{2-}$. The inset of Fig. 1A(a) shows the comparison between the experimental isotope patterns and the calculated patterns, which confirms its composition. The reactivity can be expressed in the form of the following chemical equation,

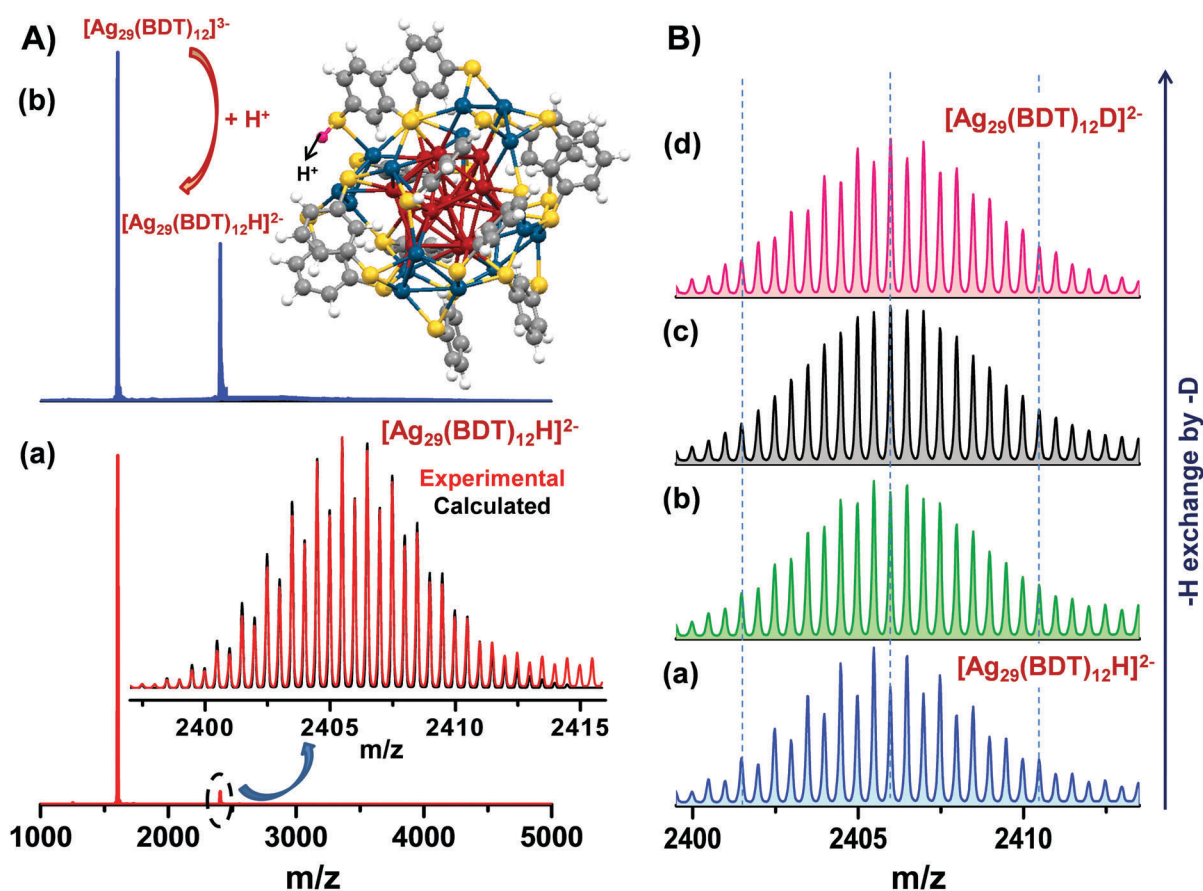
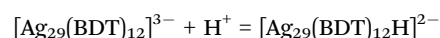


Fig. 1 (A) ESI MS of (a) $[\text{Ag}_{29}(\text{BDT})_{12}]^{3-}$ cluster in the presence of 1 mM formic acid and (b) maximum conversion of $[\text{Ag}_{29}(\text{BDT})_{12}]^{3-}$ to $[\text{Ag}_{29}(\text{BDT})_{12}\text{H}]^{2-}$ upon addition of formic acid. Inset of (a) shows the experimental and calculated isotope patterns of $[\text{Ag}_{29}(\text{BDT})_{12}\text{H}]^{2-}$ and inset of (b) shows the lowest energy DFT optimized structure of $[\text{Ag}_{29}(\text{BDT})_{12}\text{H}]^{2-}$. The proton is marked in the figure. Experimental spectrum (inset of (a) extends beyond 2415 due to overlapping contribution from other ions). (B) Isotope patterns of (a) $[\text{Ag}_{29}(\text{BDT})_{12}\text{H}]^{2-}$, (b) and (c) gradual changes in the pattern upon replacement of H by D and (d) $[\text{Ag}_{29}(\text{BDT})_{12}\text{D}]^{2-}$. See the change in the intensities of the peaks on the dotted lines in relation to the nearby peaks from (a) to (d). Color codes: red: Ag of core; blue: Ag of staples; yellow: S; grey: C; white: H atoms; and purple: proton.

However, this species should not be confused with the 2- charge state of the parent cluster as that would have only a difference of m/z 0.5 with respect to this protonated species. The isotope distribution of the species $[\text{Ag}_{29}(\text{BDT})_{12}\text{H}]^{2-}$ was also compared with the theoretical pattern of $[\text{Ag}_{29}(\text{BDT})_{12}]^{3-}$ to show the clear distinction between them (see Fig. S3, ESI†). As the cluster was sensitive to the presence of H^+ in solution, a few other control studies were also carried out by varying the solvents and the proton sources in order to get more insights about its proton capture affinity. The cluster was dissolved in a 1:1 mixture of DMF:MeOH to enhance the polarity of the medium and its mass spectrum was measured without the addition of any formic acid. In this case also, the peak for $[\text{Ag}_{29}(\text{BDT})_{12}\text{H}]^{2-}$ was observed, though at low intensity, as shown in Fig. S4A (ESI†). It was even sensitive to the proton concentration when one drop of water was added to the cluster solution in DMF (see Fig. S4B, ESI†). We also studied the feasibility of H/D exchange in the system by adding D_2O as the D^+ source and within 2 min of D_2O addition, there was a complete exchange and $[\text{Ag}_{29}(\text{BDT})_{12}\text{D}]^{2-}$ was formed. In Fig. 1B, where (a) represents the ESI MS of $[\text{Ag}_{29}(\text{BDT})_{12}\text{H}]^{2-}$, gradual changes in the distribution of the peaks of the isotope pattern start upon addition of D_2O , which is shown in (b) and (c). Finally, on complete conversion to $[\text{Ag}_{29}(\text{BDT})_{12}\text{D}]^{2-}$, there was a shift to higher mass by m/z 0.5 and this is shown in (d). H/D exchange further confirmed the binding of a proton to the cluster and hence the assignment.

Again, the cluster solutions were prepared in NH_4OAc buffer solutions of varying concentrations (0.25 M, 0.5 M and 1 M) in a

1:1 mixture of DMF and MeOH and ESI MS was measured. The conversion of $[\text{Ag}_{29}(\text{BDT})_{12}]^{3-}$ to $[\text{Ag}_{29}(\text{BDT})_{12}\text{H}]^{2-}$ increased with an increase in the concentration of NH_4OAc and finally in a solution of 1 M NH_4OAc , there was a complete conversion of the cluster to $[\text{Ag}_{29}(\text{BDT})_{12}\text{H}]^{2-}$. This was monitored by ESI MS, as shown in Fig. 2A. The decay in the relative intensity of $[\text{Ag}_{29}(\text{BDT})_{12}]^{3-}$ and the corresponding growth in the intensity of $[\text{Ag}_{29}(\text{BDT})_{12}\text{H}]^{2-}$ with an increase in the concentration of NH_4OAc are shown in Fig. 2B. There was no complexation with NH_4^+ , instead, proton transfer occurred from the reaction medium (pH of the medium was 6.8). This supports the strong proton capture tendency of the cluster. When a tertiary amine salt (NMe_4Br), which has no transferable protons on the N atom, was added, the cluster showed complexation with the $(\text{NMe}_4)^+$ group (Fig. S5, ESI†). However, in all such reactions, the absorption features of the cluster were not much affected (Fig. S6, ESI†). In the structure of the cluster, there are no free groups like $-\text{OH}$, $-\text{NH}_2$ or $-\text{COO}^-$ in the ligands that can become easily protonated. So, the proton possibly interacts at some specific site of the cluster and that results in a change in the overall charge delocalization. MS/MS studies were also carried out to gain better insight into the structure and the binding interactions (Fig. S7, ESI†).^{27,48–50} Upon increasing energy, the proton was lost and the cluster $[\text{Ag}_{29}(\text{BDT})_{12}]^{3-}$ was reformed. $[\text{Ag}_5(\text{BDT})_3]^-$ is a common fragment of $[\text{Ag}_{29}(\text{BDT})_{12}]^{3-12}$ and the proton was found to be associated with the thiolates as $[\text{Ag}_4(\text{BDT})_3\text{H}]^-$. Further, by the use of soft ionization conditions, we have observed that proton capture can occur with the intact $[\text{Ag}_{29}(\text{BDT})_{12}(\text{TPP})_4]^{3-}$ clusters that exist in solution,

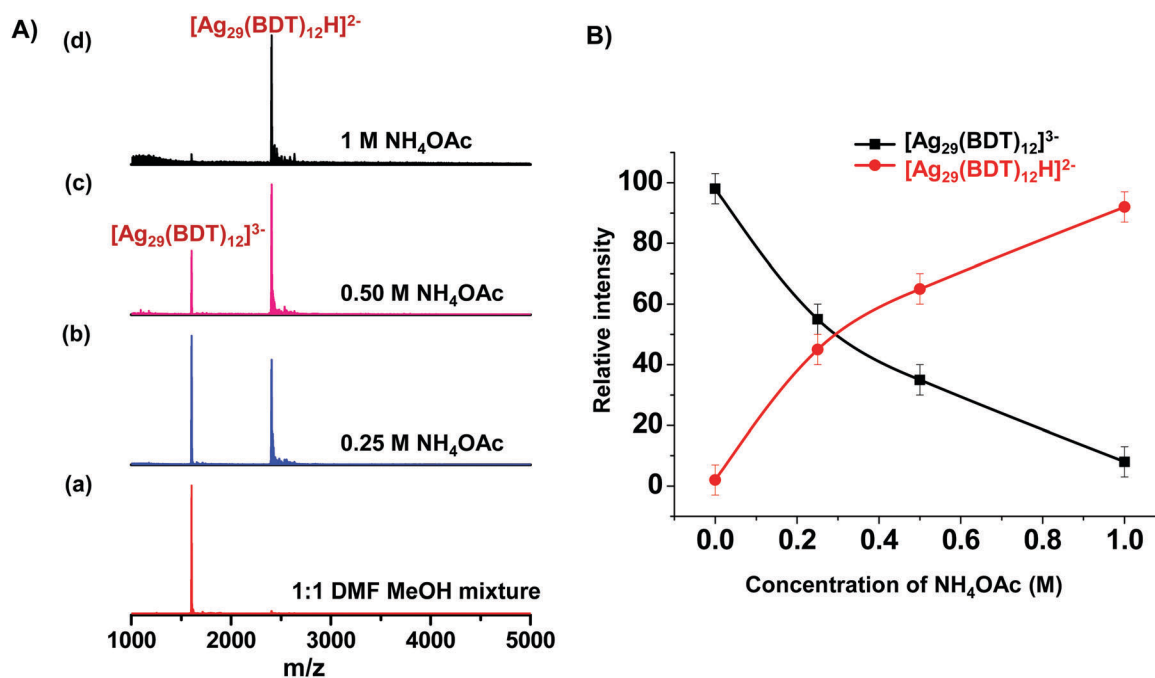


Fig. 2 (A) ESI MS of $[\text{Ag}_{29}(\text{BDT})_{12}]^{3-}$ cluster in 1:1 DMF/MeOH solution of NH_4OAc at different concentrations: (a) 0 M, (b) 0.25 M, (c) 0.5 M and (d) 1 M. The spectra show that there is an increase in the conversion of $[\text{Ag}_{29}(\text{BDT})_{12}]^{3-}$ to $[\text{Ag}_{29}(\text{BDT})_{12}\text{H}]^{2-}$ with an increase in the concentration of NH_4OAc . (B) Plot showing the decay in the relative intensities of $[\text{Ag}_{29}(\text{BDT})_{12}]^{3-}$ and growth in the relative intensities of $[\text{Ag}_{29}(\text{BDT})_{12}\text{H}]^{2-}$, respectively with an increase in the concentration of NH_4OAc .

leading to the formation of $[\text{Ag}_{29}(\text{BDT})_{12}\text{H}(\text{TPP})_n]^{2-}$ ($n = 1-4$) clusters, as shown in Fig. S8 (ESI[†]). To understand the possible structures of $[\text{Ag}_{29}(\text{BDT})_{12}\text{H}]^{2-}$, computational studies were carried out. The most stable structure is shown in the inset of Fig. 1A(b).

3.2 DFT optimized structure of $[\text{Ag}_{29}(\text{BDT})_{12}\text{H}]^{2-}$

The structure of $[\text{Ag}_{29}(\text{BDT})_{12}]^{3-}$ was optimized using the coordinates of the crystal structure from previous reports.¹¹ A proton may interact with Ag and S atoms. In the exterior shell, two types of S atoms are present, S atoms that form the Ag_3S_3 crown motifs are bonded only to Ag atoms of the staples and the other S atoms are bonded to both the core and staple Ag atoms (Fig. S9, ESI[†]). The possible structures of $[\text{Ag}_{29}(\text{BDT})_{12}\text{H}]^{2-}$ were optimized using DFT calculations and the optimized geometries are shown in Fig. S10 (ESI[†]). We first started with the attachment of a proton onto the S atoms that are bonded only to the outer shell Ag atoms in the structure of $[\text{Ag}_{29}(\text{BDT})_{12}]^{3-}$. Initially, the proton was placed in the vicinity of three S atoms of one Ag_3S_3 unit but during optimization, it was shifted towards one of them (Fig. S10A, ESI[†]) and forms a bond with S at a distance of 1.38 Å. This results in the cleavage of one of the Ag–S bonds and this Ag–S distance changes from 2.52 to 3.59 Å. The S atom retains its bonding with the other Ag atom. Next, the proton was interacted with the S atom that is connected to one of the core Ag atoms. DFT optimization suggests the formation of a bond in this case also (Fig. S10B, ESI[†]). However, the interaction of a proton at this position was less favorable. The relative energies for all the proton-bound clusters were calculated and are shown in Fig. S10 (ESI[†]). The proton attached to the S atom that is bonded only to the outer shell Ag atoms was the most stable structure. This optimized structure is shown in the inset of Fig. 1A(b) and also in the ESI[†]. The binding energy of the proton to the cluster in the most stable structure of $[\text{Ag}_{29}(\text{BDT})_{12}\text{H}]^{2-}$ is $-74.07 \text{ kcal mol}^{-1}$. The H–S bond distance (1.38 Å) is slightly higher than the normal covalent H–S bond length (1.34 Å) and subsequently the binding energy is also slightly less than the average value reported for a covalent H–S bond energy ($-86.8 \text{ kcal mol}^{-1}$).⁵¹

As the proton capture can occur with the intact $[\text{Ag}_{29}(\text{BDT})_{12}(\text{TPP})_4]^{3-}$ clusters, we have further optimized the structure of $[\text{Ag}_{29}(\text{BDT})_{12}\text{H}(\text{TPP})_4]^{2-}$ by using DFT calculations. In the presence of TPP ligands, the binding of a proton also occurs in a similar manner and the S–H bond distance (1.38 Å) is the same in both cases (Fig. S11, ESI[†]). Binding energy is also similar in both the structures $[\text{Ag}_{29}(\text{BDT})_{12}\text{H}]^{2-}$ ($-74.07 \text{ kcal mol}^{-1}$) and $[\text{Ag}_{29}(\text{BDT})_{12}\text{H}(\text{TPP})_4]^{2-}$ ($-73.92 \text{ kcal mol}^{-1}$), which suggests that the TPP ligands do not impart additional steric hindrance or play any major role in the stabilization of the proton addition to the cluster. Further, the reactivity of a cluster depends on the energy gap between its highest occupied molecular orbital (HOMO) and lowest unoccupied molecular orbital (LUMO). The interaction with the proton can alter the HOMO–LUMO energy gap. The calculated HOMO–LUMO gap decreases from 1.62 eV to 1.15 eV in the most stable structure of $[\text{Ag}_{29}(\text{BDT})_{12}\text{H}]^{2-}$. However, these HOMO–LUMO calculations are based on the ground state geometry of the clusters. Actual comparison with

the experimental optical absorption spectra requires further studies involving time dependent density functional theory (TDDFT) calculations that will consider the optical excitations.

We have not observed more than one proton binding to the cluster in our experiments. However, computationally, we have checked the effect of the addition of another proton to the structure of $[\text{Ag}_{29}(\text{BDT})_{12}\text{H}]^{2-}$. The structure of $[\text{Ag}_{29}(\text{BDT})_{12}\text{H}_2]^{-}$ was constructed by adding a proton to another equivalent S atom in the structure of $[\text{Ag}_{29}(\text{BDT})_{12}\text{H}]^{2-}$ and then optimizing it in DFT (see Fig. S12, ESI[†]). Binding energy of the second proton ($-36.20 \text{ kcal mol}^{-1}$) decreases significantly compared to that of the first proton ($-74.07 \text{ kcal mol}^{-1}$). The protons are likely to attach on the S atoms, which weakens the bonding of the –SR groups with the Ag atoms. Hence, if more protons are bound to the cluster, it might ultimately lead to degradation of the system due to significant weakening of the bonding of the thiol group with the metal core.⁵² Further, as the interaction of the protons is mainly with the S atoms of the thiol groups, this indicates that such protonation might also be possible for free-standing $\text{Ag}(\text{I})\text{SR}$ oligomers.

3.3 Reactivity with alkali metal ions

The study was extended to a series of alkali metal ions (Li^+ , Na^+ , K^+ , Rb^+ and Cs^+). While moving down the periodic table, from Li^+ to Cs^+ , the ions show increasing atomic radius, decreasing electronegativity, and increasing reactivity. The Li^+ ion is the smallest and it has a high hydration energy in the gas phase, its reduction potential is more negative than the others indicating it to be the most electropositive alkali metal. Due to such properties, there may be some difference in the reactivity of the cluster with the metal ions. However, the cluster reacted with each of these metal ions to form $[\text{Ag}_{29}(\text{BDT})_{12}\text{Li}]^{2-}$, $[\text{Ag}_{29}(\text{BDT})_{12}\text{Na}]^{2-}$, $[\text{Ag}_{29}(\text{BDT})_{12}\text{K}]^{2-}$, $[\text{Ag}_{29}(\text{BDT})_{12}\text{Rb}]^{2-}$, and $[\text{Ag}_{29}(\text{BDT})_{12}\text{Cs}]^{2-}$, respectively. Fig. 3 shows the ESI MS of the cluster in the presence of about 1 mM solutions of the respective salts. The isotope patterns of each of these peaks have been matched with the calculated patterns to confirm their composition, as shown in the insets of Fig. 3. Each of these species was subjected to MS/MS studies. The fragmentation pattern was similar to the case of $[\text{Ag}_{29}(\text{BDT})_{12}\text{H}]^{2-}$. With the increase of energy, the metal ions were lost and the cluster ion $[\text{Ag}_{29}(\text{BDT})_{12}]^{3-}$ was reformed. Along with the formation of the common fragment $[\text{Ag}_5(\text{BDT})_3]^{-}$, the alkali metal ions were found to be associated with the thiolates as $[\text{Ag}_4(\text{BDT})_3\text{M}]^{-}$ ($\text{M} = \text{Li}, \text{Na}, \text{K}, \text{Rb}, \text{Cs}$) (Fig. S13, ESI[†]). Though the dissociation pattern proposes a similarity between all these structures, significant differences are expected as compared to the structure of $[\text{Ag}_{29}(\text{BDT})_{12}\text{H}]^{2-}$ as the proton is smaller in size and also has different properties. We have studied the possible structure of one of these species, $[\text{Ag}_{29}(\text{BDT})_{12}\text{Na}]^{2-}$, by DFT calculations. Similar to the case of the proton, the alkali metal ion capture can also occur with the intact $[\text{Ag}_{29}(\text{BDT})_{12}(\text{TPP})_4]^{3-}$ clusters that exist in solution (Fig. S14, ESI[†]).

3.4 DFT optimized structure of $[\text{Ag}_{29}(\text{BDT})_{12}\text{Na}]^{2-}$

The structure of $[\text{Ag}_{29}(\text{BDT})_{12}\text{Na}]^{2-}$ was optimized in a similar manner as in the case of the proton. Interestingly, Na^+ sits

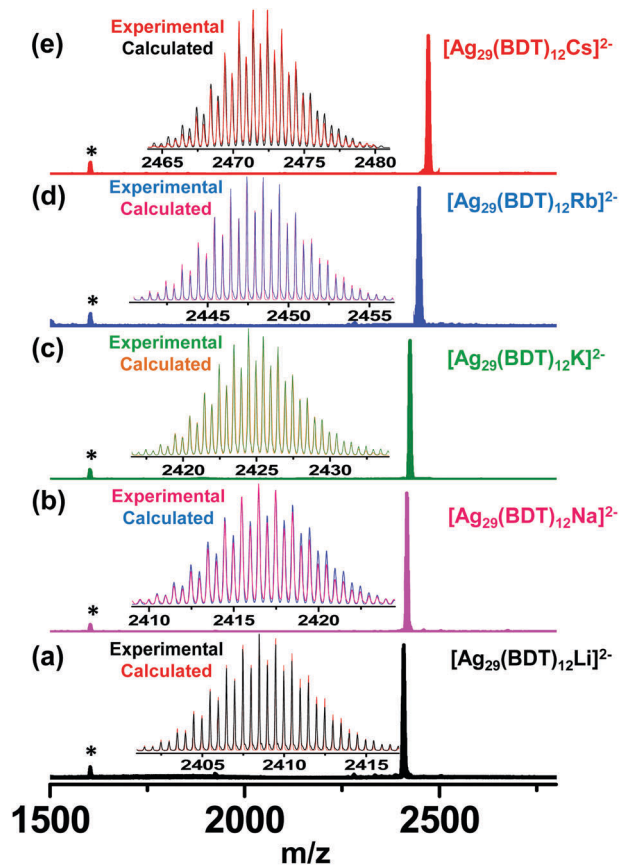


Fig. 3 ESI MS of (a) $[\text{Ag}_{29}(\text{BDT})_{12}\text{Li}]^{2-}$, (b) $[\text{Ag}_{29}(\text{BDT})_{12}\text{Na}]^{2-}$, (c) $[\text{Ag}_{29}(\text{BDT})_{12}\text{K}]^{2-}$, (d) $[\text{Ag}_{29}(\text{BDT})_{12}\text{Rb}]^{2-}$, and (e) $[\text{Ag}_{29}(\text{BDT})_{12}\text{Cs}]^{2-}$. Insets show their respective experimental and calculated isotope patterns. '*' indicates the peak for $[\text{Ag}_{29}(\text{BDT})_{12}]^{3-}$.

above the plane of three S atoms, which is in contrast to the binding pattern of the proton. The optimized structures are shown in Fig. 4, where (A) represents the DFT optimized structure with Na^+ sitting over the plane of three S atoms, one of which is connected to the core, and (B) represents the structure with Na^+ sitting over the plane of three S atoms of a Ag_3S_3 motif, all S atoms of which are bonded only to Ag atoms of the staples. The distances between Na and S range from 2.74 to 2.77 Å and 2.84 to 2.86 Å in the two cases, respectively. Na^+ also interacts with the Ag atom that resides at the center of the three S atoms at a distance of 2.99 Å in the case of structure (A), whereas it has interactions with all three Ag atoms of the outer shell at a distance of 2.97–3.03 Å in the case of the second structure (B). The structure (A) is energetically more stable, which is reflected in its lower bonding distances and interaction energies. The interaction energies are $-60.43 \text{ kcal mol}^{-1}$ and $-45.51 \text{ kcal mol}^{-1}$ for the structures (A) and (B), respectively. The strength of the interaction is weaker when compared to the proton and in the case of Na^+ , the interactions were mainly electrostatic in nature. To understand the interaction, bader charge analysis was performed on the complex, which shows that the charge on Na in the complex is $0.86e$. The interaction of a molecule with a metal ion can have several components such

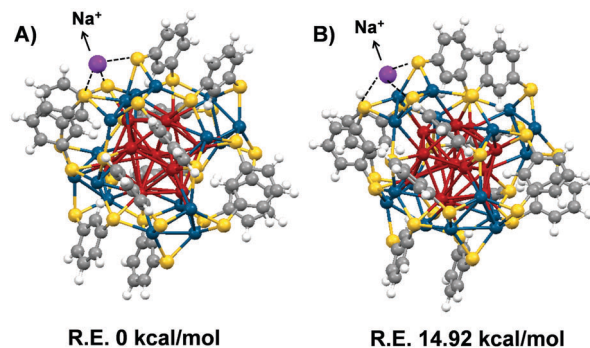


Fig. 4 DFT optimized structure of $[\text{Ag}_{29}(\text{BDT})_{12}\text{Na}]^{2-}$ with Na^+ atom sitting over the plane of three S atoms, (A) one of which is connected to a core Ag atom and (B) all of which are bonded only to Ag atoms of the staples.

as electrostatic, charge transfer and polarization. Here, the interactions were stabilized by both electrostatic and charge transfer contributions.⁵³ The calculated HOMO–LUMO gap for $[\text{Ag}_{29}(\text{BDT})_{12}\text{Na}]^{2-}$ is 1.14 eV, which is less than the HOMO–LUMO gap for $[\text{Ag}_{29}(\text{BDT})_{12}]^{3-}$ (1.62 eV), which implies that the electrostatic interaction changes the reactivity of the cluster.

A similar structure is expected for the clusters with the other alkali metal ions. Cs^+ was interacted with the cluster in a similar fashion to understand the effect of the size of the ions. The structure is similar with Cs^+ situated above the plane of three S atoms at a distance of 3.65 Å from the Ag atom, situated at the centre of the plane of the three S atoms, which is higher than that of Na^+ (2.99 Å) and this is due to the larger size of Cs^+ (Fig. S15, ESI†). The distances between Cs^+ and the neighbouring three S atoms range between 3.31 and 3.40 Å, which is also higher compared to that of Na^+ .

3.5 Separation of the dimers $[\text{Ag}_{29}(\text{BDT})_{12}\text{M}]_2^{4-}$ [M = Na, K, Rb, Cs] by ion mobility mass spectrometry (IM MS)

Cation binding is known to induce conformational changes in proteins, amino acids, drugs, carbohydrates, *etc.*^{54–59} Proton-bound and alkali-metal bound dimers^{60–64} have also been observed in several cases. Similarly, on complexation with the alkali metal ions, new metal centers are introduced into the cluster system and new interactions originate at specific sites. The cation bound species were subjected to ion mobility studies by passing them through the mobility drift tube. The changes in their structures were reflected in their drift time values (Fig. 5A). With an increase in the size of the cations ($\text{H}^+ < \text{Li}^+ < \text{Na}^+ < \text{K}^+ < \text{Rb}^+ < \text{Cs}^+$), there was a slight increase in the drift time of the monomeric species $[\text{Ag}_{29}(\text{BDT})_{12}\text{M}]^{2-}$ [M = H, Li, Na, K, Rb, Cs]. With appropriate optimization of the ion mobility conditions, dimerization was observed in some of these species. Dimers having a composition of $[\text{Ag}_{29}(\text{BDT})_{12}\text{M}]_2^{4-}$ [M = Na, K, Rb, Cs] were separated in the mobility cell and this phenomenon was selective to the nature of the cations (Fig. 5A). An optimised condition involving a trap gas flow of 10 mL min^{-1} , He gas flow of 180 mL min^{-1} and IMS gas flow of 120 mL min^{-1} was used for separating the dimers. The wave velocity and wave height were kept at 650 m s^{-1} and 35 V, respectively. The relative population of the respective monomers and dimers was

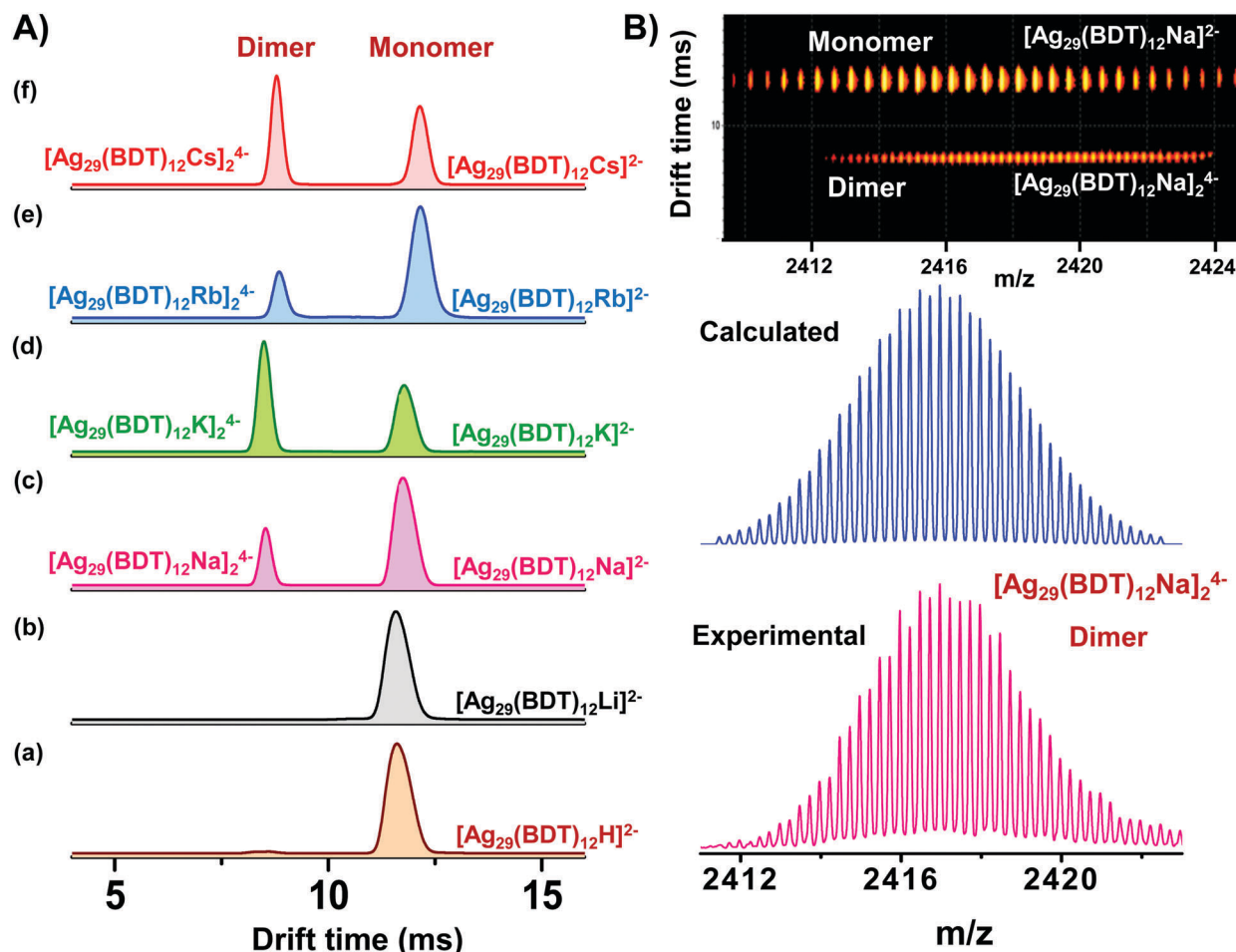


Fig. 5 (A) Drift time profile of (a) $[Ag_{29}(BDT)_{12}H]^{2-}$, (b) $[Ag_{29}(BDT)_{12}Li]^{2-}$ and dimers and monomers of (c) $[Ag_{29}(BDT)_{12}Na]_2^{4-}$, (d) $[Ag_{29}(BDT)_{12}K]_2^{4-}$, (e) $[Ag_{29}(BDT)_{12}Rb]_2^{4-}$ and (f) $[Ag_{29}(BDT)_{12}Cs]_2^{4-}$. (B) Experimental and calculated isotope patterns of the dimer $[Ag_{29}(BDT)_{12}Na]_2^{4-}$ along with the plot of drift time vs. m/z showing the separation of monomers and dimers.

specific to the instrumental conditions used. Fig. 5B shows the calculated and experimental isotope patterns of the dimer of one such species, $[Ag_{29}(BDT)_{12}Na]_2^{4-}$, along with the drift scope view showing its separation. The isotope patterns of the other dimeric species are included in the ESI[†] (Fig. S16). Dimer formation was not observed for the species containing the smaller sized cations H^+ and Li^+ . From such phenomena, it is clear that specific metal ions are required for the dimerization process to be favorable. The size of the cations may be one such critical factor. The cluster itself does not dimerize (Fig. S17, ESI[†]), dimerization is induced by the presence of cations in this case. The interactions should be strong enough to hold the two clusters together. DFT calculations revealed some changes in the structure and binding interactions between H^+ and Na^+ bound clusters, and this was reflected in their tendency towards dimerization as well. In order to form dimers, a monomer of the cluster should interact with another monomer through H^+ or Na^+ . The proton resides inside the space between the three S atoms due to its smaller size. Hence, it is not available for interacting with another cluster. Na^+ is more exposed as it is present over the plane of the three S atoms on the outer surface of the cluster. Therefore, it is available to

interact with another cluster. This explains the need for a critical size of the metal ions for forming the dimers.

A protonated benzene dimer with a sandwich like structure was reported by Jouvét *et al.*⁶⁵ In the structure of the $[Ag_{29}(BDT)_{12}]^{3-}$ cluster, the benzene rings of two BDT ligands lie in parallel orientation. So, there are additional possibilities of such sandwich protonated structures and the fact that smaller cations like H^+ and Li^+ do not form dimers might also be due to such structures remaining in competition. To consider such possibilities, we have constructed a structure of $[Ag_{29}(BDT)_{12}H]^{2-}$ with the proton sandwiched between the benzene rings of two BDT ligands and optimized it using DFT calculations. As an initial input, the proton was placed equidistant from the benzene rings of the two BDT ligands. However, in the final structure obtained after complete optimization, the proton was bound to a C atom of one of the benzene rings with a bond length of 1.13 Å, which is slightly higher than that of the usual C–H bond distance. The distance of the proton from the nearest C atom of the other benzene ring is 2.54 Å (Fig. S18, ESI[†]). This conformation with the proton sandwiched between the benzene rings of two BDT ligands is similar to that observed in the case of the protonated benzene dimer.⁶⁵ However, when compared to the structure of $[Ag_{29}(BDT)_{12}H]^{2-}$ with the

proton attached at the staple S atoms, this sandwiched structure is energetically less favourable (the structure is 20.30 kcal mol⁻¹ higher in energy than the lowest energy structure). Thus, it is verified that structures with cations sandwiched between the benzene rings are less likely to be in competition.

3.6 DFT optimized structure of the dimer [Ag₂₉(BDT)₁₂Na]₂⁴⁻

Computational studies were extended to understand the structure of the dimers. Since dimerization is induced by the metal ions, Na⁺ of one of the monomers can interact with another monomer in different ways and act as a bridge between the two clusters. The possible DFT optimized structures and the calculated relative energies are shown in Fig. 6. Na⁺ interacts with the S atoms present in another monomer. The stability of these structures is attributed to Na–S interactions. In the lowest energy structure (A), two monomers are bonded with the help of two Na⁺ ions. In another possible structure (B), only one Na⁺ participates in the dimerization process. The energy difference between the two isomeric structures is 23.86 kcal mol⁻¹. The Na–S bond distances are about 2.76–2.85 Å and 3.76 Å for structures (A) and (B), respectively. The greater number of Na–S interactions provides higher stability to structure (A). The structure of the dimers, [Ag₂₉(BDT)₁₂Na]₂⁴⁻, is very different to the structure of the dimers of Au₂₅(SR)₁₈ clusters, reported recently.²¹ While the dimerization of Au₂₅(SR)₁₈ was favored by auriphilic interaction and inter-staple bonding, in this case, dimerization is due to the incorporation of the additional metal center linking the two clusters.

3.7 Structural correlation between the monomers and the dimers from IM MS and dissociation studies

Correlation between the structures of the monomeric species, [Ag₂₉(BDT)₁₂M]₂⁴⁻ (M = H, Li, Na, K, Rb, Cs), as well as their

dimers, [Ag₂₉(BDT)₁₂M]₂⁴⁻ (M = Na, K, Rb, Cs), was clearly reflected in their drift time values. Drift time (ms) of the species was studied as a function of *m/z* for all the monomeric as well as the dimeric species (see Fig. 7A and B). As discussed earlier, with an increase in the size of the metal ions, there was an elongation of the M–S bond length, which resulted in an increase in the overall size of the cluster, and this was reflected in the increasing drift time values for the monomers and their respective dimers. The collision cross section (CCS) values of the respective monomers and dimers, measured from IM MS studies, also suggested a similar increase in the overall size of the species with an increase in the size of the metal ions (Fig. S19, ESI[†]). Monomers and dimers containing larger sized cations show a significant increase in CCS values compared to those of the protonated species. This might also be due to the fact that larger cations like Rb⁺ and Cs⁺ are not buried into the ligands and are situated away from the surface of the cluster. Dissociation studies were also carried out on the dimers. Upon increasing the collision energy (CE, instrumental units), fragmentation of the dimers to their respective monomers occurred. Drift time profiles showing the CE dependent abundances of the monomers and the dimers with increasing energy are presented in Fig. S20 (ESI[†]). Relative abundance of the monomers and the dimers are plotted as a function of the applied CE in Fig. 7C. It was observed that all the dimeric species followed a similar trend in their dissociation. At CE 30, there was about 50% dissociation of the dimers to their respective monomers, whereas, after CE 50, there was complete dissociation to the monomers. The dissociation thresholds were similar in all cases, which suggests a similarity in the structure of the dimers formed by the different metal ions.

3.8 Possibilities of interaction with other metal ions, detection of [Ag₂₉(BDT)₁₂Ag]₂⁴⁻

Similar reactivity can be extended to a range of other metal ions also. Complexation of the cluster with Ag⁺ was also observed, which leads to the formation of the cluster–metal ion adduct having a composition of [Ag₂₉(BDT)₁₂Ag]₂⁴⁻. When it was passed through the ion mobility cell, dimers of [Ag₂₉(BDT)₁₂Ag]₂⁴⁻ were also separated under similar conditions, as shown in Fig. 8. The area under the peaks of the mobilogram reflects the relative abundance of the respective species. The experimental and calculated isotope patterns of the dimers and the monomers are shown in the insets of Fig. 8, which confirm their composition. The drift time of the [Ag₂₉(BDT)₁₂Ag]₂⁴⁻ monomer is 11.40 ms and that of the [Ag₂₉(BDT)₁₂Ag]₂⁴⁻ dimer is 8.57 ms, which are much lower drift time values than expected from the drift time *vs.* *m/z* correlation of the species [Ag₂₉(BDT)₁₂M]₂⁴⁻, as shown in Fig. 7A and B. Thus, it is evident that this correlation between drift time (ms) and *m/z* might not be valid in the case of Ag⁺ or other monovalent cations. With an increase in the mass of the alkali metals, there is also an increase in their size from Li⁺ to Cs⁺. The structures of [Ag₂₉(BDT)₁₂M]₂⁴⁻ may vary depending on the nature of the metal. This implies that Ag cation capture may lead to a very different bonding scheme and incorporation of Ag within the Ag core can also occur. However, the exact structure of [Ag₂₉(BDT)₁₂Ag]₂⁴⁻ cannot be predicted only from the drift

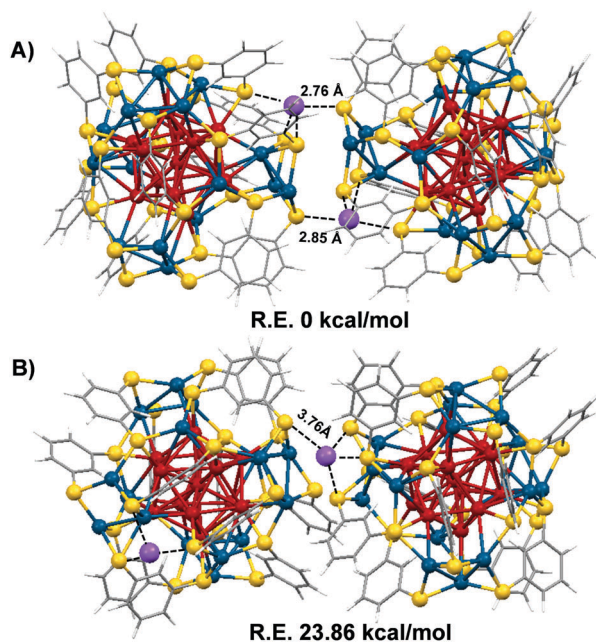


Fig. 6 DFT optimized structures of the dimer, [Ag₂₉(BDT)₁₂Na]₂⁴⁻, with two monomers bonded with (A) two Na⁺ and (B) only one Na⁺.

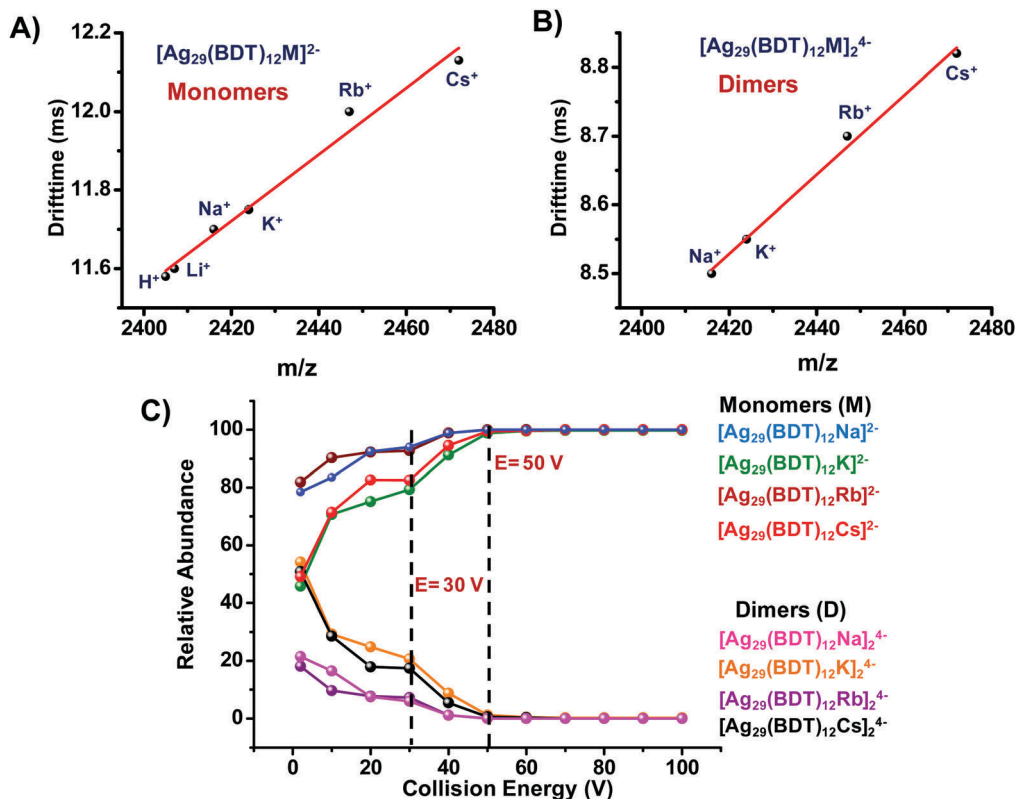


Fig. 7 Plot of drift time vs. m/z of (A) monomeric species $[\text{Ag}_{29}(\text{BDT})_{12}\text{M}]^{2-}$ ($\text{M} = \text{H}, \text{Li}, \text{Na}, \text{K}, \text{Rb}, \text{Cs}$) and (B) dimeric species $[\text{Ag}_{29}(\text{BDT})_{12}\text{M}]_2^{4-}$ ($\text{M} = \text{Na}, \text{K}, \text{Rb}, \text{Cs}$); (C) collision energy resolved fragmentation curves of the dimers and the monomers.

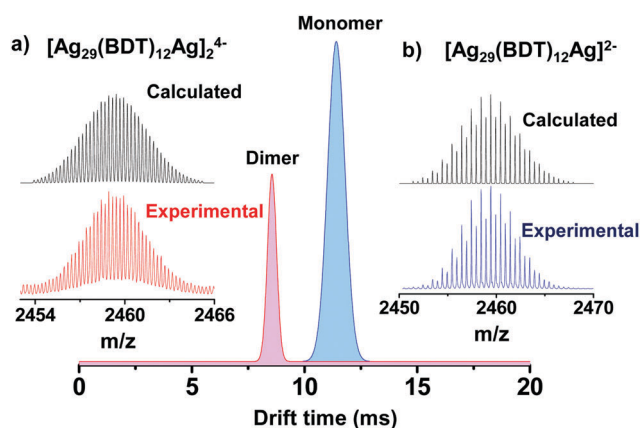


Fig. 8 Drift time profile showing the separation of the dimers and the monomers of $[\text{Ag}_{29}(\text{BDT})_{12}\text{Ag}]^{2-}$. Insets show the calculated and experimental isotope patterns of (a) the dimer $[\text{Ag}_{29}(\text{BDT})_{12}\text{Ag}]_2^{4-}$ and (b) the monomer $[\text{Ag}_{29}(\text{BDT})_{12}\text{Ag}]^{2-}$.

time vs. m/z correlation. For complete structural elucidation, detailed studies are required, which are areas for further investigation.

4. Conclusions

In summary, we have explored the reactivity of a proton (H^+) and alkali metal ions (Li^+ , Na^+ , K^+ , Rb^+ and Cs^+) with the

$[\text{Ag}_{29}(\text{BDT})_{12}]^{3-}$ cluster. The structural changes resulting from the binding of the ions have been studied and alkali metal-bound dimers of the cluster have been separated by IM MS. While this study helps to identify the structural changes and interactions that can favour the formation of cluster aggregates, such transient states can also be related to the chemical reactivity of the cluster. The sensitivity of the cluster towards H^+ can be used to quantify the proton concentration in organic solvents. As affinity towards H^+ gives an idea regarding the gas-phase basicity of a molecule, the acid base chemistry involving the cluster can be explored in more detail. Due to the strong tendency of the cluster to bind to cations, it may be used in the detection of alkali metal ions like Na^+ , K^+ , etc.

Conflicts of interest

There are no conflicts to declare.

Acknowledgements

P. C. thanks the Council of Scientific and Industrial Research (CSIR) for a research fellowship. A. B. thanks IIT Madras for an Institute Postdoctoral fellowship. S. K. M. thanks DST-INSPIRE for his research fellowship. A. N. thanks IIT Madras for an Institute Doctoral fellowship. G. P. thanks IIT Madras for an Institute Post-Doctoral fellowship. We thank the Department of

Science and Technology, Government of India for continuous support of our research program.

References

- R. Jin, C. Zeng, M. Zhou and Y. Chen, *Chem. Rev.*, 2016, **116**, 10346–10413.
- A. Mathew and T. Pradeep, *Part. Part. Syst. Charact.*, 2014, **31**, 1017–1053.
- I. Chakraborty and T. Pradeep, *Chem. Rev.*, 2017, **117**, 8208–8271.
- N. Goswami, Q. Yao, T. Chen and J. Xie, *Coord. Chem. Rev.*, 2016, **329**, 1–15.
- J. Fang, B. Zhang, Q. Yao, Y. Yang, J. Xie and N. Yan, *Coord. Chem. Rev.*, 2016, **322**, 1–29.
- M. Zhu, C. M. Aikens, F. J. Hollander, G. C. Schatz and R. Jin, *J. Am. Chem. Soc.*, 2008, **130**, 5883–5885.
- H. Qian, W. T. Eckenhoff, Y. Zhu, T. Pintauer and R. Jin, *J. Am. Chem. Soc.*, 2010, **132**, 8280–8281.
- Y. Levi-Kalisman, P. D. Jadzinsky, N. Kalisman, H. Tsunoyama, T. Tsukuda, D. A. Bushnell and R. D. Kornberg, *J. Am. Chem. Soc.*, 2011, **133**, 2976–2982.
- H. Yang, Y. Wang, H. Huang, L. Gell, L. Lehtovaara, S. Malola, H. Hakkinen and N. Zheng, *Nat. Commun.*, 2013, **4**, 2422.
- C. P. Joshi, M. S. Bootharaju, M. J. Alhilaly and O. M. Bakr, *J. Am. Chem. Soc.*, 2015, **137**, 11578–11581.
- L. G. Abdul Halim, M. S. Bootharaju, Q. Tang, S. Del Gobbo, R. G. Abdul Halim, M. Eddaoudi, D.-E. Jiang and O. M. Bakr, *J. Am. Chem. Soc.*, 2015, **137**, 11970–11975.
- P. Chakraborty, A. Baksi, E. Khatun, A. Nag, A. Ghosh and T. Pradeep, *J. Phys. Chem. C*, 2017, **121**, 10971–10981.
- A. Baksi, S. R. Harvey, G. Natarajan, V. H. Wysocki and T. Pradeep, *Chem. Commun.*, 2016, **52**, 3805–3808.
- A. Baksi, A. Ghosh, S. K. Mudedla, P. Chakraborty, S. Bhat, B. Mondal, K. R. Krishnadas, V. Subramanian and T. Pradeep, *J. Phys. Chem. C*, 2017, **121**, 13421–13427.
- M. R. Ligare, E. S. Baker, J. Laskin and G. E. Johnson, *Chem. Commun.*, 2017, **53**, 7389–7392.
- K. R. Krishnadas, A. Ghosh, A. Baksi, I. Chakraborty, G. Natarajan and T. Pradeep, *J. Am. Chem. Soc.*, 2016, **138**, 140–148.
- K. R. Krishnadas, A. Baksi, A. Ghosh, G. Natarajan and T. Pradeep, *Nat. Commun.*, 2016, **7**, 13447.
- B. Yoon, W. D. Luedtke, R. N. Barnett, J. Gao, A. Desireddy, B. E. Conn, T. Bigioni and U. Landman, *Nat. Mater.*, 2014, **13**, 807.
- A. Som, I. Chakraborty, T. A. Maark, S. Bhat and T. Pradeep, *Adv. Mater.*, 2016, **28**, 2827–2833.
- M. De Nardi, S. Antonello, D.-E. Jiang, F. Pan, K. Rissanen, M. Ruzzi, A. Venzo, A. Zoleo and F. Maran, *ACS Nano*, 2014, **8**, 8505–8512.
- A. Baksi, P. Chakraborty, S. Bhat, G. Natarajan and T. Pradeep, *Chem. Commun.*, 2016, **52**, 8397–8400.
- F. Lanucara, S. W. Holman, C. J. Gray and C. E. Eyers, *Nat. Chem.*, 2014, **6**, 281–294.
- Y. Zhong, S.-J. Hyung and B. T. Ruotolo, *Expert Rev. Proteomics*, 2012, **9**, 47–58.
- A. A. Shvartsburg, S. Y. Noskov, R. W. Purves and R. D. Smith, *Proc. Natl. Acad. Sci. U. S. A.*, 2009, **106**, 6495–6500.
- M. Zhou, S. Dagan and V. H. Wysocki, *Angew. Chem., Int. Ed.*, 2012, **51**, 4336–4339.
- R. S. Quintyn, M. Zhou, S. Dagan, J. Finke and V. H. Wysocki, *Int. J. Ion Mobility Spectrom.*, 2013, **16**, 133–143.
- R. S. Quintyn, S. R. Harvey and V. H. Wysocki, *Analyst*, 2015, **140**, 7012–7019.
- S. Daly, C. M. Choi, A. Zavras, M. Krstić, F. Chirot, T. U. Connell, S. J. Williams, P. S. Donnelly, R. Antoine, A. Giuliani, V. Bonačić-Koutecký, P. Dugourd and R. A. J. O'Hair, *J. Phys. Chem. C*, 2017, **121**, 10719–10727.
- A. Soleilhac, F. Bertorelle, C. Comby-Zerbino, F. Chirot, N. Calin, P. Dugourd and R. Antoine, *J. Phys. Chem. C*, 2017, **121**, 27733–27740.
- G. Hu, Q. Tang, D. Lee, Z. Wu and D.-E. Jiang, *Chem. Mater.*, 2017, **29**, 4840–4847.
- R. Araake, K. Sakadani, M. Tada, Y. Sakai and Y. Ohki, *J. Am. Chem. Soc.*, 2017, **139**, 5596–5606.
- M. S. Bootharaju, R. Dey, L. E. Gevers, M. N. Hedhili, J.-M. Basset and O. M. Bakr, *J. Am. Chem. Soc.*, 2016, **138**, 13770–13773.
- R. S. Dhayal, W. E. van Zyl and C. W. Liu, *Acc. Chem. Res.*, 2016, **49**, 86–95.
- A. Zavras, G. N. Khairallah, T. U. Connell, J. M. White, A. J. Edwards, R. J. Mulder, P. S. Donnelly and R. A. J. O'Hair, *Inorg. Chem.*, 2014, **53**, 7429–7437.
- A. Moser, K. Range and D. M. York, *J. Phys. Chem. B*, 2010, **114**, 13911–13921.
- E. P. L. Hunter and S. G. Lias, *J. Phys. Chem. Ref. Data*, 1998, **27**, 413–656.
- S. G. Lias, J. F. Liebman and R. D. Levin, *J. Phys. Chem. Ref. Data*, 1984, **13**, 695–808.
- F. Wang, S. Ma, D. Zhang and R. G. Cooks, *J. Phys. Chem. A*, 1998, **102**, 2988–2994.
- Z. Wu, C. Fenselau and R. Graham Cooks, *Rapid Commun. Mass Spectrom.*, 1994, **8**, 777–780.
- M. R. A. Blomberg and P. E. M. Siegbahn, *Biochim. Biophys. Acta*, 2006, **1757**, 969–980.
- H. Ishikita and K. Saito, *J. R. Soc., Interface*, 2014, **11**, 20130518.
- D. Jacquemin, J. Zuniga, A. Requena and J. P. Ceron-Carrasco, *Acc. Chem. Res.*, 2014, **47**, 2467–2474.
- J. J. Warren and J. M. Mayer, *Biochemistry*, 2015, **54**, 1863–1878.
- J. J. Mortensen, L. B. Hansen and K. W. Jacobsen, *Phys. Rev. B: Condens. Matter Mater. Phys.*, 2005, **71**, 035109.
- J. Enkovaara, C. Rostgaard, J. J. Mortensen, J. Chen, M. Dulak, L. Ferrighi, J. Gavnholt, C. Glinsvad, V. Haikola, H. A. Hansen, H. H. Kristoffersen, M. Kuisma, A. H. Larsen, L. Lehtovaara, M. Ljungberg, O. Lopez-Acevedo, P. G. Moses, J. Ojanen, T. Olsen, V. Petzold, N. A. Romero, J. Stausholm-Møller, M. Strange, G. A. Tritsaridis, M. Vanin, M. Walter, B. Hammer, H. Häkkinen, G. K. H. Madsen, R. M. Nieminen, J. K. Nørskov, M. Puska, T. T. Rantala, J. Schiøtz,

- K. S. Thygesen and K. W. Jacobsen, *J. Phys.: Condens. Matter*, 2010, **22**, 253202.
- 46 J. P. Perdew, K. Burke and M. Ernzerhof, *Phys. Rev. Lett.*, 1996, **77**, 3865–3868.
- 47 A. H. Larsen, M. Vanin, J. J. Mortensen, K. S. Thygesen and K. W. Jacobsen, *Phys. Rev. B: Condens. Matter Mater. Phys.*, 2009, **80**, 195112.
- 48 R. G. Cooks, *J. Mass Spectrom.*, 1995, **30**, 1215–1221.
- 49 E. R. Williams, L. Fang and R. N. Zare, *Int. J. Mass Spectrom. Ion Processes*, 1993, **123**, 233–241.
- 50 G. E. Johnson, T. Priest and J. Laskin, *Chem. Sci.*, 2014, **5**, 3275–3286.
- 51 S. W. Benson, *J. Chem. Educ.*, 1965, **42**, 502.
- 52 L. Gell and H. Häkkinen, *J. Phys. Chem. C*, 2015, **119**, 10943–10948.
- 53 B. Sharma, Y. I. Neela and G. Narahari Sastry, *J. Comput. Chem.*, 2016, **37**, 992–1004.
- 54 T. G. Flick, I. D. G. Campuzano and M. D. Bartberger, *Anal. Chem.*, 2015, **87**, 3300–3307.
- 55 L. Chen, Y. Q. Gao and D. H. Russell, *J. Phys. Chem. A*, 2012, **116**, 689–696.
- 56 A. Memboeuf, K. Vekey and G. Lendvay, *Eur. J. Mass Spectrom.*, 2011, **17**, 33–46.
- 57 S. Lee, T. Wyttenbach, G. von Helden and M. T. Bowers, *J. Am. Chem. Soc.*, 1995, **117**, 10159–10160.
- 58 Y. Seo, M. R. Schenauer and J. A. Leary, *Int. J. Mass Spectrom.*, 2011, **303**, 191–198.
- 59 Y. Huang and E. D. Dodds, *Anal. Chem.*, 2013, **85**, 9728–9735.
- 60 W. Fu, J. Xiong, M. J. Lecours, P. J. J. Carr, R. A. Marta, E. Fillion, T. McMahon, V. Steinmetz and W. S. Hopkins, *J. Mol. Spectrosc.*, 2016, **330**, 194–199.
- 61 B. Yang, R. R. Wu and M. T. Rodgers, *J. Am. Soc. Mass Spectrom.*, 2015, **26**, 1469–1482.
- 62 M. Tsuge, J. Kalinowski, R. B. Gerber and Y.-P. Lee, *J. Phys. Chem. A*, 2015, **119**, 2651–2660.
- 63 B. Yang and M. T. Rodgers, *Phys. Chem. Chem. Phys.*, 2014, **16**, 16110–16120.
- 64 L. Wu, E. C. Meurer, B. Young, P. Yang, M. N. Eberlin and R. G. Cooks, *Int. J. Mass Spectrom.*, 2004, **231**, 103–111.
- 65 S. Chakraborty, R. Omidyan, I. Alata, I. B. Nielsen, C. Dedonder, M. Broquier and C. Jouvet, *J. Am. Chem. Soc.*, 2009, **131**, 11091–11097.